Deposited via The University of Leeds.

Article:

1   **Skeletal myofiber VEGF deficiency leads to mitochondrial, structural, and**

2   **contractile alterations in mouse diaphragm**

3

4   Daniel T Cannon[1]*, Lukas Rodewohl[2]*, Volker Adams[3], Ellen C Breen[4], T Scott Bowen[5]

5

6   [1]School of Exercise & Nutritional Sciences, San Diego State University

7   [2]Department of Internal Medicine and Cardiology, Universität Leipzig Herzzentrum

8   [3]Department of Internal Medicine and Cardiology, Technische Universität Dresden

9   [4]Department of Medicine, University of California, San Diego

10   [5]School of Biomedical Sciences, Faculty of Biological Sciences, University of Leeds

11   *equal contribution

12

13   **Author Contributions**

14   Concept and design: DTC, ECB, TSB. Data acquisition: DTC, LR, ECB, TSB. Data

15   analysis: DTC, LR, TSB. Data interpretation: DTC, LR, VA, ECB, TSB. Figure preparation:

16   DTC, LR, TSB. Manuscript drafting: DTC, LR, TSB. Critical Revision: DTC, LR, VA, ECB,

17   TSB. All authors approved the final version.

18

19   **Corresponding Author**

20   T. Scott Bowen

21   School of Biomedical Sciences

22   University of Leeds, Leeds, LS2 9JT

23   t.s.bowen@leeds.ac.uk

24

25   **Running title:** Myofiber VEGF deletion induces diaphragm dysfunction

26

27   **Key words:** diaphragm, muscle, fatigue, mitochondria

Abstract

Diaphragm dysfunction accompanies cardiopulmonary disease and impaired oxygen delivery. Vascular endothelial growth factor (VEGF) regulates oxygen delivery through angiogenesis, capillary maintenance, and contraction-induced perfusion. We hypothesized that myofiber-specific VEGF deficiency contributes to diaphragm weakness and fatigability. Diaphragm protein expression, capillarity and fiber morphology, mitochondrial respiration and hydrogen peroxide (H_2O_2) generation, and contractile function were compared between adult mice with conditional gene ablation of skeletal myofiber VEGF (SkmVEGF$^{-/-}$; n=12) and littermate controls (n=13). Diaphragm VEGF protein was ~50 % lower in SkmVEGF$^{-/-}$ than littermate controls (1.45 ± 0.65 vs. 3.04 ± 1.41 pg/total protein; P=0.001). This was accompanied by an ~15% impairment in maximal isometric specific force ($F_{[1,23]} = 15.01$, P=0.001) and a trend for improved fatigue resistance (P=0.053). Mean fiber cross-sectional area and type I fiber cross-sectional area were lower in SkmVEGF$^{-/-}$ by ~40 % and ~25% (P<0.05). Capillary-to-fiber ratio was also lower in SkmVEGF$^{-/-}$ by ~40% (P<0.05), thus capillary density was not different. Sarcomeric actin expression was ~30% lower in SkmVEGF$^{-/-}$ (P<0.05), while myosin heavy chain and MAFbx were similar (measured via immunoblot). Mitochondrial respiration, citrate synthase activity, PGC-1α, and HIF-1α were not different in SkmVEGF$^{-/-}$ (P>0.05). However mitochondrial-derived reactive oxygen species (ROS) flux was lower in SkmVEGF$^{-/-}$ (P=0.0003). In conclusion, myofiber-specific VEGF gene deletion resulted in a lower capillary-to-fiber ratio, type I fiber atrophy, actin loss, and contractile dysfunction in the diaphragm. In contrast, mitochondrial respiratory function was preserved alongside lower ROS generation, which may play a compensatory role to preserve fatigue resistance in the diaphragm.

Abstract word count: 244 (250 max).

53

New and Noteworthy (75 words max).

Diaphragm weakness is a hallmark of diseases where oxygen delivery is compromised. Vascular endothelial growth factor (VEGF) modulates muscle perfusion, however it remains unclear whether VEGF deficiency contributes to the onset of diaphragm dysfunction.

Conditional skeletal myofiber VEGF gene ablation impaired diaphragm contractile function and resulted in type I fiber atrophy, a lower number of capillaries per fiber, and contractile protein content. Mitochondrial function was similar and ROS flux was lower. Diaphragm VEGF deficiency may contribute to the onset of respiratory muscle weakness.

Introduction

Respiratory muscle weakness develops in many clinical conditions, such as acute critical illness, chronic cardiopulmonary disorders, and in aging (23). In particular, impairments to the main muscle of respiration, the diaphragm, contributes substantially to pulmonary complications and poor clinical outcomes in patients (18, 33). However, the mechanisms that induce diaphragm weakness and effective rescue treatments remain poorly resolved. Most clinical disorders associated with diaphragm dysfunction are characterized by abnormal microvasculature and O_2 delivery (49) (e.g., critical illness, chronic heart failure, chronic obstructive pulmonary disease; COPD). Abnormalities in the O_2 transport system may be a key mechanism for triggering the onset of diaphragm weakness (23). Vascular endothelial growth factor (VEGF) is a transmembrane glycoprotein that is requisite for blood vessel development and maintenance in all mammalian organs. VEGF is a family of 5 growth factors (VEGF-A, VEGF-B, VEGF-C, VEGF-D, PGF) that have various roles during embryonic/adult tissue development and maintenance. However, VEGF-A (referred hereafter as VEGF) is the most predominant form in the majority of tissues/organs in adults. In addition to signal transduction for angiogenesis, VEGF is critical for stem cell recruitment, maintenance of vulnerable barriers (i.e. lung, nephron and kidney cells), and protection of neural tissue (10, 51).

VEGF plays a critical role in locomotor skeletal muscle structure and function and these variables impact whole-organism functions, such as exercise tolerance (26, 50). Further, skeletal muscle remodeling following exercise training is highly dependent on VEGF being properly expressed in a variety of tissues, including skeletal myofibers (16, 25). VEGF is down-regulated in leg muscle samples taken from patients with diseases characterized by abnormalities in O_2 supply, such as in COPD (5). In contrast, the role of VEGF expression in the diaphragm remains poorly characterized and whether low VEGF contributes to diaphragm contractile dysfunction is unknown. Interestingly, in rats undergoing mechanical ventilation where the diaphragm

90 undergoes arrest to induce severe fiber weakness, VEGF is reduced by around two-fold (11, 17).

91 However in conditions with high mechanical respiratory loading, such as COPD (2) or under

92 hypoxic conditions (46), VEGF mRNA expression in the diaphragm is elevated. Thus, it seems

93 that in conditions characterized by diaphragm disuse such as in critical illness, a reduction in

94 VEGF expression may contribute towards respiratory muscle weakness. The mechanisms that

95 underpin diaphragm dysfunction have been suggested to include fiber atrophy (due to an

96 imbalance in protein synthesis/degradation), elevated reactive oxygen species (ROS), an

97 oxidative to glycolytic fiber type transition, and mitochondrial dysfunction (23, 41).

98

99 Based upon the importance of VEGF in locomotor skeletal muscle during adaptation to exercise

100 training and various pathologies, we aimed to measure whether VEGF deficiency modulates

101 diaphragm contractile function, capillarity, fiber structure, and mitochondrial bioenergetics. Given

102 that diaphragm tissue demonstrates a high degree of cellular abnormalities in a variety of

103 diseases (6, 8, 9, 31, 32), we hypothesized that low myofiber VEGF impairs diaphragm contractile

104 function and is accompanied by fiber remodeling and mitochondrial functional deficits including

105 capillary regression, fiber atrophy, shifts from oxidative to glycolytic fiber types, and reduced

106 maximal mitochondrial oxygen flux with increased ROS generation.

107

Materials and Methods

Animals and Study Design

We measured diaphragm biochemistry, structure, and contractile function in adult mice with conditional deletion of the VEGF-A gene in skeletal myofibers (SkmVEGF$^{-/-}$). To achieve this, we maintained and bred mice homozygous for the VEGF*LoxP* transgene (22) with mice heterogeneous for HSA-Cre-ER^{T2} (44). Animals were housed in a pathogen-free vivarium in plastic cages, with a 12:12 hr light:dark cycle, and fed a standard chow diet (Harlan Tekland 8604, Madison, WI) with water *ad libitum*. Conditional myofiber-specific deletion of VEGF was initiated at 10 weeks of age (body weight ~20 g) using a tamoxifen-inducible HSA-Cre-ER^{T2} system in the VEGF*LoxP* mice on a C57BL/6J background (16). Male SkmVEGF$^{-/-}$ mice (n=12) were compared to floxed wild type (WT) controls (n=13) that did not express cre recombinase (HSA-Cre-ER$^{T2-/-}$). All mice received tamoxifen (1 mg/day i.p.) for 5 consecutive d (D0-D4). Following completion of the tamoxifen treatment period and sufficient time for VEGF expression to be decreased, mice were anesthetized on day 21 (D21) with inhaled isoflurane vaporized in 100% O_2 and killed through removing the major organs. Our protocol was approved by the University of California, San Diego, Animal Care and Use Committee and was conducted in accordance to guidelines outlined by the NIH's *Guide for the Care and Use of Laboratory Animals*.

Genotyping

The presence of HSA-Cre-ER^{T2} transgene was measured by PCR from tail DNA and forward 5′-CTAGAGCCTGTTTTGCACGTTC-3′ and reverse primers 5′-TGCAAGTTGAATAACCGGAAA-3′. The conditions during cycling were a 2-min polymerase activation incubation at 95°C, 35 cycles of 30 s denaturation at 94°C, 30 s annealing at 52.1°C, 60 s elongation at 72°C, followed by one 8-min elongation at 72°C.

133   *Diaphragm Dissection and Contractile Function*

134   The diaphragm was excised through a laparotomy and thoracotomy. The right costal diaphragm

135   muscle was divided for measurement of mitochondrial function and the remainder immediately

136   snap-frozen in liquid N_2 for later biochemical analyses. The left costal diaphragm muscle was

137   prepared in a Krebs-Hanseleit buffer solution (120.5 mM NaCl, 4.8 mM KCl, 1.2 mM $MgSO_4$, 1.2

138   mM NaH_2PO_4, 20.4 mM $NaHCO_3$, 1.6 mM $CaCl_2$, 10 mM dextrose, 1 mM pyruvate at a pH of 7.4)

139   and a muscle bundle (~3 mg) connected from rib to central tendon was dissected, sutured (size

140   4.0), and mounted horizontally in a buffer-filled organ bath at room temperature equilibrated with

141   $95\%O_2$-$5\%CO_2$. The suture connected to the rib was secured to a hook in the organ bath while

142   the tendon was tied to an adjustable-length force transducer (Model 920CS, DMT, Aarhus, DK).

143   The muscle was stimulated via platinum electrodes with a supramaximal current (500-ms train

144   duration; 0.25-ms monophasic pulses) via a high-power stimulator (Model S88, Grass Medical

145   Instruments, Quincy, MA). The muscle bundle was set at an optimal length equivalent to the

146   maximal twitch force produced and a 15-min equilibration period followed. A force-frequency

147   protocol was then performed at 1, 15, 30, 50, 80, 120, 150, and 300 Hz, respectively, separated

148   with 1-min rest intervals. Following a 5-min period in which muscle length was measured using a

149   digital micrometer, the muscle underwent a fatigue protocol over 5 min (40 Hz every 2 s with a

150   500-ms train duration). The muscle was subsequently detached, trimmed free from rib and

151   tendon, blotted dry on filter paper, and weighed. Muscle force (N) was normalized to muscle cross-

152   sectional area (cm^2) by dividing muscle mass (g) by the product of optimal length (cm) and

153   estimated muscle density (1.06 g/cm^3) (13), which allowed specific force in N/cm^2 to be calculated.

154

155   *Mitochondrial function*

156   Dissected diaphragm tissue (~5-10 mg) was placed immediately in preservation solution at 4°C.

157   Preservation medium (BIOPS) contained 10 mM Ca^{2+}EGTA buffer, 20 mM imidazole, 50 mM K^+-

158   4-morpholineothanesulfonic acid (MES), 0.5 mM dithiothreitol, 6.56 mM $MgCl_2$, 5.77 mM ATP, 15

159   mM phosphocreatine and a pH of 7.1. Fiber bundles (each approximately 0.5 to 1 mg) were

160   transferred to a plastic culture dish and kept in BIOPS at 4°C. The bundles were mechanically

161   separated using sharp forceps and a dissection microscope (Leica, DE). The bundles were

162   permeabilized with a 30 min incubation in saponin (50 µg/ml) dissolved in BIOPS at 4°C. Tissues

163   were washed of saponin for 10 min in respiration medium at 4°C. Fiber bundles were weighed to

164   the nearest µg using an ultrabalance (UMX2, Mettler-Toledo, Greifensee, CH) and transferred

165   into a calibrated respirometer (Oxygraph 2k, OROBOROS INSTRUMENTS, Innsbruck, AT)

166   containing 2 ml of media in each chamber. Respirometry and fluorometry was performed in

167   duplicate at 37°C in stirred media (MiR05+Cr) containing 0.5 mM EGTA, 3 mM $MgCl_2$, 60 mM K-

168   lactobionate, 20 mM taurine, 10 mM KH_2PO_4, 20 mM HEPES, 110 mM sucrose, 20 mM creatine,

169   and 1 g/l BSA essentially fatty acid free, adjusted to pH 7.1. $[O_2]$ in the media was kept between

170   300–500 µM.

171

172   A substrate-uncoupler-inhibitor-titration (SUIT) protocol (37) included: 10 mM glutamate and 2

173   mM malate to support electron entry through complex I (GM; '*LEAK*' state), 5 mM ADP to stimulate

174   oxidative phosphorylation ('OXPHOS_CI' state), 10 mM succinate to maximize convergent

175   electron   flux   at   the   Q-junction   (ADP+S;   OXPHOS_CI+II),   carbonyl   cyanide-3-

176   chlorophenylhydrazone (CCCP) titrated in 0.5 µM steps to achieve maximal uncoupled respiration

177   for measurement of electron transport system capacity ('ETS' state), 0.5 µM rotenone to inhibit

178   complex I (Rot; ETS_CII). The flux control ratio for OXPHOS was calculated as

179   (OXPHOS_CI/ETS) and (OXPHOS_CI+II/ETS). OXPHOS coupling efficiency was calculated as

180   (1-LEAK/OXPHOS_CI+II). The substrate control ratio for succinate was calculated as

181   (OXPHOS_CI+II/OXPHOS_CI).

182

183   In parallel to respirometry, the green fluorescence-sensor of the O2k-Fluo LED2-Module

184   (OROBOROS) and the Amplex UltraRed assay was used to measure hydrogen peroxide (H_2O_2)

185   production during of the respiratory states – an index of total mitochondrial ROS production (27).

186   Amplex UltraRed (AmR; 10µM), horseradish peroxidase (HRP; 1 U/mL) and superoxide

187   dismutase (SOD; 5 U/mL) were injected prior to addition substrates. AmR is oxidized by H_2O_2 in

188   the presence of HRP and allows for an excitation/emission at 563 and 587 nm. [H_2O_2] was

189   determined by calibrating to a series of injections of 0.1 µM H_2O_2 using a 40uM stock solution

190   made fresh daily.

191

192   *Muscle Biochemistry*

193   VEGF protein in diaphragm tissue was quantified by ELISA and normalized to total protein, in

194   accordance to the manufacturer's instructions (VEGF Mouse ELISA, R&D Systems, La Jolla, CA).

195   For western blotting, frozen muscle samples were homogenized in relaxing buffer (90 HEPES,

196   126 KCl, 36 NaCl, 1 MgCl, 50 EGTA, 8 ATP, 10 creatine phosphate, in mmol/L at pH 7.4)

197   containing a protease inhibitor mix (Inhibitor mix M, Serva, Heidelberg, Germany), and sonicated

198   for 10 cycles (Sonoplus GM70, Bandelin Electronics, Berlin Germany), with protein content of the

199   homogenate subsequently determined (BCA assay, Pierce, Bonn, Germany). Citrate synthase

200   activity (a marker of mitochondrial content) was assessed at room temperature, as previously

201   described (6, 8, 9, 31, 32). Diaphragm homogenates (5 - 20 µg) mixed with loading buffer (126

202   mM Tris-HCl, 20% glycerol, 4% SDS, 1.0% 2-mercaptoethanol, 0.005% bromophenol blue; pH

203   6.8) were separated by SDS-polyacrylamide gel electrophoresis. Proteins were transferred to a

204   polyvinylidene fluoride membrane (PVDF) and incubated overnight at 4°C with the following

205   primary antibodies for the contractile proteins of myosin heavy chain (MyHC; 1/1000, Sigma-

206   Aldrich, Taufkirchen, Germany), and sarcomeric actin (1/500; Sigma-Aldrich, Taufkirchen,

207   Germany), the signaling proteins of PGC1-α (1/200, Santa Cruz, Heidelberg, Germany) and HIF1-

208   α (1/200, Santa Cruz, Heidelberg, Germany), and the stress-related proteins MAFbx (1/2000;

209   Eurogentec, Seraing, Belgium) and NADPH oxidase subunit gp91[phox] (1/1000; Abcam,

210   Cambridge, UK). Membranes were subsequently incubated with a horseradish peroxidase-

8

conjugated secondary antibody and specific bands visualized by enzymatic chemiluminescence

(Super Signal West Pico, Thermo Fisher Scientific Inc., Bonn, Germany) and densitometry

quantified using a 1D scan software package (Scanalytics Inc., Rockville, USA). Blots were then

normalized to the loading control GAPDH (1/30000; HyTest Ltd, Turku, Finland), which we

confirmed was not different between experimental groups. All data are presented as fold change

relative to control group.

Histology

Liquid-nitrogen isopentane frozen diaphragm sections prepared for cryosectioning were cut at 10

μm, mounted on glass cover slips, and incubated overnight at 4°C in antibody diluent (Dako,

Hamburg, Germany) with primary antibodies against myosin heavy chain type I fibers (M8421,

1/400; Sigma, Taufkirchen, Germany) or laminin (1/200; Sigma, Taufkirchen, Germany). After

washing with TBST, sections were incubated with fluorescently-conjugated (Alexa 488)

secondary antibodies for 1 h, further washed, and then visualized under a fluorescent microscope.

Images were captured at x5 magnification and merged to allow fiber morphology to be determined

using imaging software (Analysis Five, Olympus, Münster, Germany), which included ~300-500

fibers in a muscle area of ~500,000 μm^2 (i.e., ~40-50% of the total muscle section). Stained fibers

(bright green) were taken as type I, unstained fibers (black) as type II, with fiber boundaries

demarcated in red. In addition, capillaries were stained with lectin specific to endothelial cells

using rhodamine-conjugated Griffonia simplicifolia lectin-1 (1:250 dilution; Vector Laboratories

Ltd, Peterborough, UK), with the capillary-to-fiber (C/F) ratio (number of capillaries to number of

fibers) and capillary density (CD; number of capillaries per mm^2 of muscle tissue) calculated

alongside the mean fiber cross sectional area (FCSA). Images were captured at x40

magnification, which included ~100 fibers in a muscle area of ~120,000 μm^2 (i.e., ~15% of the

total muscle section).

237 *Statistical analyses*

238 Means were compared, where appropriate, with t-tests. Diaphragm muscle contractile function

239 data were analyzed using a two-factor repeated measures ANOVA (contraction time × genotype

240 and contraction frequency × genotype). Mitochondrial function data were analyzed using a two-

241 factor repeated measures ANOVA (respiratory state × genotype). Data are presented as mean ±

242 SD, and, where appropriate, the 95% confidence interval (CI_{95}) is included.

243

Results

In this conditional VEGF deficiency mouse model, we confirmed VEGF protein levels were lower

in the diaphragm of SkmVEGF$^{-/-}$ mice compared to WT mice by ~50% (1.45±0.65 vs. 3.04±1.41

pg/total protein; P=0.001).

248

Contractile function

Specific force generated by diaphragm fiber bundles was impaired following VEGF deletion by

~15% in SkmVEGF$^{-/-}$ compared to WT mice (F[1,23] = 15.01, P=0.001; main effect of genotype),

which occurred at both low and high stimulation frequencies ranging from 15 to 300 Hz (Fig 1A).

Similarly, there was a rightward shift in the normalized force frequency relationship (F[1,23] =

2.98, P=0.045; interaction), with relative forces lower between 30 - 120 Hz in SkmVEGF$^{-/-}$

diaphragm fiber bundles (Fig. 1B). In contrast, fatigue resistance tended to be higher in

SkmVEGF$^{-/-}$ compared to WT mice during the fatigue protocol (F[1,23] = 4.15, P=0.053; main

effect of genotype), such that relative force tended to be ~10% higher throughout the repeated

contractions (Fig. 1C). Twitch kinetics remained unaltered following VEGF deletion, with no

differences (P>0.05) between WT and SkmVEGF$^{-/-}$ mice in terms of time to peak tension (TPT;

43±7 vs. 42±3 ms, respectively) and half-relaxation time (HRT; 60±17 vs. 63±16 ms, respectively).

261

Muscle structure and protein expression

The C/F ratio was ~40% lower in SkmVEGF$^{-/-}$ compared to WT mice (P=0.008; Fig. 2A). In

contrast, the CD remained unchanged between groups (P>0.05; Fig. 2B) which can be explained

by the scale-dependent consequence of VEGF deletion lowering mean FCSA in parallel (Fig. 2C;

P=0.023). Representative muscle sections from WT and SkmVEGF$^{-/-}$ are presented in Fig. 2D-E.

Fiber proportion for type I slow and type II fast myosin heavy chain isoforms were not different

268   between SkmVEGF$^{-/-}$ and WT mice (P=0.455; Fig. 2F), with type I fibers representing ~10 % of

269   overall fiber population. In contrast, however, type I fiber cross-sectional area was lower by ~25

270   % in SkmVEGF$^{-/-}$ compared to WT mice (P=0.027; Fig. 2G). No difference was detected in type

271   II fiber cross-sectional area between the groups (P=0.786; Fig. 2G). While no difference was

272   observed between groups for MyHC expression (P=0.429; Fig. 3A), the smaller type I fiber size

273   corresponded to an ~30% lower level of the key contractile protein actin (P=0.011; Fig. 3B). We

274   subsequently measured key proteins known to be involved in fiber atrophy signaling, but found

275   no differences between groups in relation to the key E3 ligase MAFBx (P=0.189; Fig. 4A) and

276   major ROS source NADPH oxidase (P=0.091; Fig. 4B). We also probed for protein expression of

277   key upstream regulatory proteins in the VEGF signaling cascade, but found no differences in

278   protein expression of HIF-1α (P=0.417; Fig. 4C) and PGC-1α (P=0.176; Fig. 4D).

279

280   *Mitochondrial function*

281   Diaphragm mitochondrial O_2 consumption was not different between SkmVEGF$^{-/-}$ and WT (F[1,80]

282   = 0.85, P=0.36, Fig 5A), nor was an interaction present (respiratory state × genotype: F[4,80] =

283   0.1, P=0.98, Fig 5A). However, H_2O_2 production was lower in SkmVEGF$^{-/-}$ vs WT (F[1,75] = 14.57,

284   P=0.0003, Fig 5B), with particular differences observed at OXPHOS_CI+II and ETS_CII

285   respiratory states. OXPHOS coupling efficiency, the ratio of free to total OXPHOS capacity, was

286   not different between SkmVEGF$^{-/-}$ and WT (Fig 5C). There were no differences (P>0.05) in the

287   flux control ratios (FCR) for ADP-stimulated respiration (Fig 5D-E) or in the substrate control ratio

288   (SCR) for succinate (Fig 5F). Citrate synthase activity was also not different (P>0.05) between

289   WT and SkmVEGF$^{-/-}$ mice (8.38±0.73 vs. 8.20±0.96 µmol/min/mg protein, respectively).

290

Discussion

291 **Discussion**

292 We found that myofiber-specific VEGF deficient mice produce reduced specific tension in the

293 diaphragm accompanied by a lower C/F ratio, fiber atrophy and loss of sarcomeric actin content.

294 While the mechanisms linking VEGF signaling to diaphragm weakness remain unclear, we

295 suggest it may be related to the lower number of capillaries supplying each fiber. This could limit

296 oxygen and nutrient availability and affect contractile function via tissue hypoxia, inflammation,

297 and/or protein homeostasis (23). Interestingly, diaphragmatic mitochondrial function and content

298 were maintained in VEGF deficient mice and mitochondrial-derived ROS generation was lower.

299 These findings suggest that vascular dysfunction may lead to metabolic compensation in

300 myofibers that manifests as improved fatigue resistance measured in the absence of neural or

301 vascular systems.

302

303 ***Myofiber-VEGF deletion leads to diaphragm weakness***

304 Conditional gene deletion of skeletal myofiber-specific VEGF in adult mice reduced VEGF protein

305 levels by ~50%. While other cells, including endothelial cells, macrophage stem cells and

306 fibroblast express VEGF, myofibers are the major source of VEGF in skeletal muscle (50). Rather

307 than life-long VEGF gene ablation, conditional deletion provides a more clinically relevant model

308 to investigate whether diaphragm VEGF deficiency is linked to respiratory muscle weakness in

309 adult patients. The reduction in diaphragm VEGF levels were similar to that reported previously

310 in life-long skeletal myofiber targeted VEGF gene ablated (~60% reduction) 20 week old mice

311 (50). Life-long VEGF deficiency reduces diaphragm capillarity by around 40%, and this reduction

312 in capillaries was almost two-fold greater than that observed in locomotor muscles in this same

313 mouse line (50). We observed a similar trend in the present study. Conditional VEGF gene-

314 deletion induced in adult mice resulted in an ~40% lower C/F ratio in the diaphragm. However, in

315 contrast to mice with life-long loss of the VEGF gene, locomotor skeletal muscle capillaries are

316 stable when VEGF gene deletion is initiated in adult mice (16, 26).

317

While low VEGF levels are associated with conditions where diaphragm dysfunction is developed

such as mechanical ventilation (11, 17), a direct link had not been previously explored. Given the

diaphragm's high degree of sensitivity when homeostasis is challenged (6, 8, 9, 31, 32), we

anticipated low VEGF expression would impair diaphragm contractile function. A major finding of

our current study, therefore, was confirming that VEGF deficiency impairs isometric specific forces

by ~15% in the diaphragm. These functional differences are similar to that observed in patients

and experimental animal models where diaphragm fiber function is impaired, such as in

mechanical ventilation, critical illness, and heart failure (24, 31, 40). The contractile dysfunction

was present at both low (15-30 Hz) and high (120-300 Hz) stimulation frequencies, which

indicates that low VEGF-dependent signaling could impact a range of respiratory movements,

such as resting and exercising ventilation in addition to acute respiratory exacerbations involving

airway clearance.

330

Our data add important knowledge to indicate that respiratory muscle shows a substantial degree

of sensitivity to VEGF ablation. This is not surprising given the diaphragm shows a high sensitivity

to dysfunction compared to the limbs when challenged by disease states such as heart failure

(53), systemic hypertension (8), and pulmonary hypertension (14). Thus, the onset of diaphragm

weakness may represent an early marker of disease. The mechanism(s) is likely underpinned by

the diaphragm's persistent contraction pattern, which renders it highly susceptible to early

changes in mechanical loading (possibly related to pulmonary/acid-base disturbance) and/or

delivery of oxygen, nutrients, inflammatory cytokines, and ROS (23). Deficient skeletal myofiber

VEGF levels are also linked to whole-body reductions in exercise tolerance (26, 50), and our data

provide support that respiratory muscle weakness may be a contributing factor.

341

342

343 ***Mechanisms of VEGF-induced diaphragm weakness***

344 The mechanism(s) by which VEGF deficiency induced diaphragm contractile dysfunction remains

345 unclear. Our data confirmed impaired force generation at both low and high stimulation

346 frequencies in isolated fiber bundles concomitant with a rightward shift in the normalized force-

347 frequency relationship. Impaired forces at the low stimulation frequencies and the rightward shift

348 in the normalized force-frequency relationship in VEGF deficient diaphragm fibers could be

349 interpreted as a result of a slow-to-fast fiber type switch and/or alterations in calcium handling

350 (i.e., more rapid Ca^{2+} release/reuptake dynamics). However, we found no changes between

351 groups in terms of fiber type or twitch kinetics, which would argue against such mechanisms

352 acting. However, we did find that protein expression of sarcomeric actin was ~25% lower in the

353 diaphragm of SkmVEGF^{-/-} mice, which could directly limit cross-bridge cycling thus limiting force

354 generating capacity. It remains unclear why we observed a preferential loss of actin compared to

355 myosin. A disproportionate loss between the major contractile proteins is not uncommon and this

356 has been reported in various conditions including critical illness myopathy, immobilization, and

357 microgravity (21, 35). Under conditions of VEGF deficiency, therefore, various mechanisms may

358 be induced in the diaphragm including the preferential degradation of actin (following specific

359 targeting of numerous activated E3 ligases), impaired transcription and synthesis of actin, and/or

360 an imbalance in protein turnover rates between actin and myosin (21, 35).

361

362 The lower actin content was also a likely factor underlying atrophy preferentially observed in type

363 I fibers in the diaphragm of SkmVEGF^{-/-} mice. The reason for why we observed a preferential fiber

364 type I atrophy in VEGF deficient skeletal muscle remains unclear, but it may be consequent to

365 type I fibers having a more rich capillary supply than type II fibers. Therefore, type I fibers may be

366 more susceptible to contractile protein loss (and thus atrophy) under conditions associated with

367 VEGF deficiency that severely impair capillary maintenance [e.g., cigarette smoke exposure; (34,

368 52)]. Interestingly, loss of thin filaments may increase the maximal shortening velocity (V_{max}) even

15

369 without a change in MyHC (42). Without a measure of V_{max}, however, we can only speculate at

370 this point.

371

372 It is important to note that it remains unclear how much this loss of actin actually contributed to

373 the observed contractile weakness/type I fiber atrophy given the small proportion of type I fibers

374 present in mouse diaphragm. Nonetheless, in other diseases where O_2 delivery is impaired, such

375 as heart failure and COPD, reduced actin content in combination with muscle dysfunction and

376 atrophy are present (7, 30, 47). In muscle wasting following dexamethasone treatment or cigarette

377 exposure in mice, VEGF protein expression is also reduced (4). In combination, these findings

378 suggest VEGF may play a critical role in modulating protein homeostasis. However, we wish to

379 note a few limitations in our methodology, which include not distinguishing between the type II

380 fiber subtypes (a, x, b) and use of a low salt buffer to assess levels of MyHC and actin where total

381 abundance may not be accurately reflected if incompletely solubilized (43).

382

383 The signaling pathways responsible for protein loss and fiber atrophy in VEGF deficiency remain

384 unclear, but likely include an upregulation in protein degradation and/or a downregulation in

385 protein synthesis in muscle with insufficient supply of O_2. Given that conditional VEGF ablation

386 led to around a ~40% lower C/F ratio and as previous data have shown it can also impair muscle

387 perfusion (26, 50), it is possible that VEGF deficiency in muscle induces tissue hypoxia to activate

388 proteolytic pathways (15). It is important to note that this is speculative, as we do not have a

389 measure of diaphragm tissue hypoxia *in vivo* from the current study. Nonetheless, as protein

390 levels of the key E3 ligase atrogene MAFbx were not different between WT and SkmVEGF^{-/-} mice

391 suggests diaphragm VEGF deficiency may upregulate other key atrophic pathways associated

392 with contractile protein degradation (e.g., calpain, caspase-3, MuRF1, or increased ubiquitin

393 proteasome activity; (7, 30, 48)) or via inhibition of protein synthesis (e.g., Akt, mTOR, p70S6K

16

394 (45)). Future investigation into the role VEGF exerts over various protein synthesis/degradation

395 signaling molecules may therefore prove worthwhile.

396

397 Elevated ROS in the diaphragm in disease can also stimulate protein degradation (45) and induce

398 post-translational oxidative contractile protein modifications (9). However, as our ROS measures

399 of mitochondrial as well as transmembrane NADPH oxidase were not elevated in SkmVEGF$^{-/-}$,

400 with both known to be strong mediators of diaphragm weakness (1), this argues against VEGF

401 deficiency inducing diaphragm weakness via a ROS-related mechanism. However, an activity-

402 based assay of NADPH oxidase should be considered for future experiments. We also probed

403 upstream regulators involved in the VEGF signaling cascade for potential compensatory

404 adaptations to the VEGF deficiency. Both HIF-1α and PGC-1α independently stimulate VEGF (3),

405 with VEGF generally secreted by the transcription factor HIF-1α in response to hypoxic conditions

406 (19) and by the transcriptional coactivator PGC-1α in response to exercise (29). Both HIF-1α and

407 PGC-1α signaling in diaphragm tissue were not impacted in the present study indicating they do

408 not form part of a compensatory response to VEGF deficiency.

409
410 ***VEGF deletion does not impact diaphragm mitochondrial respiration***

411 Mitochondrial impairments are developed in diseases associated with diaphragm dysfunction (38,

412 40). However, in our study *in situ* mitochondrial O_2 consumption was not impacted. Neither

413 mitochondrial content (as assessed by citrate synthase) nor the coupling efficiency or respiratory

414 capacity were different under VEGF deficiency. Whether the fiber atrophy that occurred following

415 VEGF deficiency acted as a compensatory mechanism to maintain mitochondrial respiratory

416 function remains unclear but seems a reasonable suggestion. For example, in response to

417 derangements in muscle perfusion, a lower muscle size may help maintain adequate O_2 diffusion

418 between capillary and myocyte (26).

419

420   In contrast, mitochondrial-derived ROS flux was lower following VEGF ablation. The mechanisms

421   underlying lower mitochondrial ROS flux in SkmVEGF$^{-/-}$ mice remains uncertain, but it could be

422   related to a higher anti-oxidant enzyme capacity. For example, a compensatory increase in

423   oxidative enzyme activity (i.e., citrate synthase, β-HAD) occurs in both locomotor and diaphragm

424   muscle in mice with VEGF deficiency from birth (36) and in the gastrocnemius following

425   conditional deletion (16). As a shift towards greater muscle oxidative capacity is commonly

426   associated with increased anti-oxidant enzyme activities (e.g., superoxide dismutase, glutathione

427   peroxidase, catalase) (39), this could be a plausible explanation for why mitochondrial ROS flux

428   may be lower. However our current data showed citrate synthase activity remained unchanged.

429

430   High mitochondrial ROS production is particularly common in conditions associated with

431   diaphragm weakness, such as heart failure (28) and mechanical ventilation (40). Surprisingly, we

432   found that mitochondrial-derived ROS flux was lower in VEGF deficient diaphragm fibers. As

433   NADPH oxidase, a cytosolic ROS marker, was also not different between groups, our data

434   indicate that diaphragm weakness induced by VEGF deficiency is unlikely to be mediated by

435   elevated oxidative stress. SkmVEGF$^{-/-}$ mice may have been better protected against ROS-

436   induced muscle fatigue, as increased ROS production during repeated contractions inhibits force

437   generation (12). Interestingly, improvements in relative fatigue of the diaphragm *in vitro* are also

438   present in disease (31), which suggests the SkmVEGF$^{-/-}$ mouse model may closely reflect

439   pathological states and thus mirror adaptations to that often observed after long-term endurance

440   training (39). However, the observation of this improved fatigue resistance may be dependent on

441   the *in vitro* muscle fatigue protocol employed. Using a "matched-stimulus" rather than "matched-

442   initial specific force" protocol, healthy (or control) diaphragm fibers generate higher absolute

443   forces initially and throughout to induce an apparent more rapid fatigue (20, 31). Therefore, the

444   fatigue protocol employed in our study may explain why relative fatigue resistance was higher in

445   mice with VEGF deficiency and extrapolation of these findings should be interpreted with caution.

446

Conclusions

448 Skeletal myofiber-specific VEGF deletion resulted in diaphragm contractile dysfunction that was

449 accompanied by lower CF ratio, smaller type I fibers, lower sarcomeric actin protein, and lower

450 mitochondrial ROS generation. Whether differences in type I fiber size, capillarity, and ROS

451 generation compensated to protect mitochondrial respiratory function remains unclear. Deficient

452 diaphragm VEGF levels may be a contributing factor to the onset of diaphragm dysfunction and

453 provide a viable treatment target for patients afflicted with respiratory muscle weakness.

454

471

References

1.	**Ahn B, Beharry AW, Frye GS, Judge AR, and Ferreira LF**. NAD(P)H oxidase subunit p47phox is elevated, and p47phox knockout prevents diaphragm contractile dysfunction in heart failure. *Am J Physiol Lung Cell Mol Physiol* 309: L497-505, 2015.

2.	**Alexopoulou C, Mitrouska I, Arvanitis D, Tzanakis N, Chalkiadakis G, Melissas J, Zervou M, and Siafakas N**. Vascular-specific growth factor mRNA levels in the human diaphragm. *Respiration* 72: 636-641, 2005.

3.	**Arany Z, Foo SY, Ma Y, Ruas JL, Bommi-Reddy A, Girnun G, Cooper M, Laznik D, Chinsomboon J, Rangwala SM, Baek KH, Rosenzweig A, and Spiegelman BM**. HIF-independent regulation of VEGF and angiogenesis by the transcriptional coactivator PGC-1alpha. *Nature* 451: 1008-1012, 2008.

4.	**Barel M, Perez OA, Giozzet VA, Rafacho A, Bosqueiro JR, and do Amaral SL**. Exercise training prevents hyperinsulinemia, muscular glycogen loss and muscle atrophy induced by dexamethasone treatment. *Eur J Appl Physiol* 108: 999-1007, 2010.

5.	**Barreiro E, Schols AM, Polkey MI, Galdiz JB, Gosker HR, Swallow EB, Coronell C, Gea J, and project EiC**. Cytokine profile in quadriceps muscles of patients with severe COPD. *Thorax* 63: 100-107, 2008.

6.	**Bowen TS, Aakeroy L, Eisenkolb S, Kunth P, Bakkerud F, Wohlwend M, Ormbostad AM, Fischer T, Wisloff U, Schuler G, Steinshamn S, Adams V, and Bronstad E**. Exercise Training Reverses Extrapulmonary Impairments in Smoke-exposed Mice. *Medicine and science in sports and exercise* 49: 879-887, 2017.

7.	**Bowen TS, Adams V, Werner S, Fischer T, Vinke P, Brogger MN, Mangner N, Linke A, Sehr P, Lewis J, Labeit D, Gasch A, and Labeit S**. Small-molecule inhibition of MuRF1 attenuates skeletal muscle atrophy and dysfunction in cardiac cachexia. *Journal of cachexia, sarcopenia and muscle* 8: 939-953, 2017.

8.	**Bowen TS, Eisenkolb S, Drobner J, Fischer T, Werner S, Linke A, Mangner N, Schuler G, and Adams V**. High-intensity interval training prevents oxidant-mediated diaphragm muscle weakness in hypertensive mice. *FASEB journal : official publication of the Federation of American Societies for Experimental Biology* 31: 60-71, 2017.

9.	**Bowen TS, Mangner N, Werner S, Glaser S, Kullnick Y, Schrepper A, Doenst T, Oberbach A, Linke A, Steil L, Schuler G, and Adams V**. Diaphragm muscle weakness in mice is early-onset post-myocardial infarction and associated with elevated protein oxidation. *J Appl Physiol (1985)* 118: 11-19, 2015.

10.	**Breen EC**. VEGF in biological control. *Journal of cellular biochemistry* 102: 1358-1367, 2007.

11.	**Bruells CS, Maes K, Rossaint R, Thomas D, Cielen N, Bleilevens C, Bergs I, Loetscher U, Dreier A, Gayan-Ramirez G, Behnke BJ, and Weis J**. Prolonged

mechanical ventilation alters the expression pattern of angio-neogenetic factors in a pre-clinical rat model. *PLoS One* 8: e70524, 2013.

12. **Cheng AJ, Yamada T, Rassier DE, Andersson DC, Westerblad H, and Lanner JT**. Reactive oxygen/nitrogen species and contractile function in skeletal muscle during fatigue and recovery. *The Journal of physiology* 594: 5149-5160, 2016.

13. **Close RI**. Dynamic properties of mammalian skeletal muscles. *Physiol Rev* 52: 129-197, 1972.

14. **de Man FS, van Hees HW, Handoko ML, Niessen HW, Schalij I, Humbert M, Dorfmuller P, Mercier O, Bogaard HJ, Postmus PE, Westerhof N, Stienen GJ, van der Laarse WJ, Vonk-Noordegraaf A, and Ottenheijm CA**. Diaphragm muscle fiber weakness in pulmonary hypertension. *Am J Respir Crit Care Med* 183: 1411-1418, 2011.

15. **de Theije CC, Langen RC, Lamers WH, Schols AM, and Kohler SE**. Distinct responses of protein turnover regulatory pathways in hypoxia- and semistarvation-induced muscle atrophy. *Am J Physiol Lung Cell Mol Physiol* 305: L82-91, 2013.

16. **Delavar H, Nogueira L, Wagner PD, Hogan MC, Metzger D, and Breen EC**. Skeletal myofiber VEGF is essential for the exercise training response in adult mice. *American journal of physiology Regulatory, integrative and comparative physiology* 306: R586-595, 2014.

17. **DeRuisseau KC, Shanely RA, Akunuri N, Hamilton MT, Van Gammeren D, Zergeroglu AM, McKenzie M, and Powers SK**. Diaphragm unloading via controlled mechanical ventilation alters the gene expression profile. *Am J Respir Crit Care Med* 172: 1267-1275, 2005.

18. **Dres M, Dube BP, Mayaux J, Delemazure J, Reuter D, Brochard L, Similowski T, and Demoule A**. Coexistence and Impact of Limb Muscle and Diaphragm Weakness at Time of Liberation from Mechanical Ventilation in Medical Intensive Care Unit Patients. *Am J Respir Crit Care Med* 195: 57-66, 2017.

19. **Ferrara N, Gerber HP, and LeCouter J**. The biology of VEGF and its receptors. *Nat Med* 9: 669-676, 2003.

20. **Ferreira LF, Moylan JS, Gilliam LA, Smith JD, Nikolova-Karakashian M, and Reid MB**. Sphingomyelinase stimulates oxidant signaling to weaken skeletal muscle and promote fatigue. *Am J Physiol Cell Physiol* 299: C552-560, 2010.

21. **Fitts RH, Riley DR, and Widrick JJ**. Physiology of a microgravity environment invited review: microgravity and skeletal muscle. *J Appl Physiol (1985)* 89: 823-839, 2000.

22. **Gerber HP, Hillan KJ, Ryan AM, Kowalski J, Keller GA, Rangell L, Wright BD, Radtke F, Aguet M, and Ferrara N**. VEGF is required for growth and survival in neonatal mice. *Development* 126: 1149-1159, 1999.

23.   **Greising SM, Ottenheijm CAC, O'Halloran KD, and Barreiro E**. Diaphragm plasticity in aging and disease: therapies for muscle weakness go from strength to strength. *J Appl Physiol (1985)* 125: 243-253, 2018.

24.   **Hooijman PE, Beishuizen A, Witt CC, de Waard MC, Girbes AR, Spoelstra-de Man AM, Niessen HW, Manders E, van Hees HW, van den Brom CE, Silderhuis V, Lawlor MW, Labeit S, Stienen GJ, Hartemink KJ, Paul MA, Heunks LM, and Ottenheijm CA**. Diaphragm muscle fiber weakness and ubiquitin-proteasome activation in critically ill patients. *Am J Respir Crit Care Med* 191: 1126-1138, 2015.

25.   **Huey KA, Smith SA, Sulaeman A, and Breen EC**. Skeletal myofiber VEGF is necessary for myogenic and contractile adaptations to functional overload of the plantaris in adult mice. *J Appl Physiol (1985)* 120: 188-195, 2016.

26.   **Knapp AE, Goldberg D, Delavar H, Trisko BM, Tang K, Hogan MC, Wagner PD, and Breen EC**. Skeletal myofiber VEGF regulates contraction-induced perfusion and exercise capacity but not muscle capillarity in adult mice. *American journal of physiology Regulatory, integrative and comparative physiology* 311: R192-199, 2016.

27.   **Krumschnabel G, Fontana-Ayoub M, Sumbalova Z, Heidler J, Gauper K, Fasching M, and Gnaiger E**. Simultaneous high-resolution measurement of mitochondrial respiration and hydrogen peroxide production. *Methods Mol Biol* 1264: 245-261, 2015.

28.   **Laitano O, Ahn B, Patel N, Coblentz PD, Smuder AJ, Yoo JK, Christou DD, Adhihetty PJ, and Ferreira LF**. Pharmacological targeting of mitochondrial reactive oxygen species counteracts diaphragm weakness in chronic heart failure. *J Appl Physiol (1985)* 120: 733-742, 2016.

29.   **Leick L, Hellsten Y, Fentz J, Lyngby SS, Wojtaszewski JF, Hidalgo J, and Pilegaard H**. PGC-1alpha mediates exercise-induced skeletal muscle VEGF expression in mice. *Am J Physiol Endocrinol Metab* 297: E92-103, 2009.

30.   **Levine S, Biswas C, Dierov J, Barsotti R, Shrager JB, Nguyen T, Sonnad S, Kucharchzuk JC, Kaiser LR, Singhal S, and Budak MT**. Increased proteolysis, myosin depletion, and atrophic AKT-FOXO signaling in human diaphragm disuse. *Am J Respir Crit Care Med* 183: 483-490, 2011.

31.   **Mangner N, Bowen TS, Werner S, Fischer T, Kullnick Y, Oberbach A, Linke A, Steil L, Schuler G, and Adams V**. Exercise Training Prevents Diaphragm Contractile Dysfunction in Heart Failure. *Medicine and science in sports and exercise* 48: 2118-2124, 2016.

32.   **Mangner N, Weikert B, Bowen TS, Sandri M, Hollriegel R, Erbs S, Hambrecht R, Schuler G, Linke A, Gielen S, and Adams V**. Skeletal muscle alterations in chronic heart failure: differential effects on quadriceps and diaphragm. *Journal of cachexia, sarcopenia and muscle* 6: 381-390, 2015.

583   33.   **Meyer FJ, Borst MM, Zugck C, Kirschke A, Schellberg D, Kubler W, and Haass**
584   **M**. Respiratory muscle dysfunction in congestive heart failure: clinical correlation and
585   prognostic significance. *Circulation* 103: 2153-2158, 2001.

586   34.   **Nogueira L, Trisko BM, Lima-Rosa FL, Jackson J, Lund-Palau H, Yamaguchi**
587   **M, and Breen EC**. Cigarette smoke directly impairs skeletal muscle function through
588   capillary regression and altered myofibre calcium kinetics in mice. *The Journal of*
589   *physiology* 596: 2901-2916, 2018.

590   35.   **Ochala J, Gustafson AM, Diez ML, Renaud G, Li M, Aare S, Qaisar R,**
591   **Banduseela VC, Hedstrom Y, Tang X, Dworkin B, Ford GC, Nair KS, Perera S, Gautel**
592   **M, and Larsson L**. Preferential skeletal muscle myosin loss in response to mechanical
593   silencing in a novel rat intensive care unit model: underlying mechanisms. *The Journal of*
594   *physiology* 589: 2007-2026, 2011.

595   36.   **Olfert IM, Howlett RA, Tang K, Dalton ND, Gu Y, Peterson KL, Wagner PD,**
596   **and Breen EC**. Muscle-specific VEGF deficiency greatly reduces exercise endurance in
597   mice. *The Journal of physiology* 587: 1755-1767, 2009.

598   37.   **Pesta D, and Gnaiger E**. High-resolution respirometry: OXPHOS protocols for
599   human cells and permeabilized fibers from small biopsies of human muscle. *Methods Mol*
600   *Biol* 810: 25-58, 2012.

601   38.   **Picard M, Jung B, Liang F, Azuelos I, Hussain S, Goldberg P, Godin R,**
602   **Danialou G, Chaturvedi R, Rygiel K, Matecki S, Jaber S, Des Rosiers C, Karpati G,**
603   **Ferri L, Burelle Y, Turnbull DM, Taivassalo T, and Petrof BJ**. Mitochondrial
604   dysfunction and lipid accumulation in the human diaphragm during mechanical
605   ventilation. *Am J Respir Crit Care Med* 186: 1140-1149, 2012.

606   39.   **Powers SK, Criswell D, Lawler J, Martin D, Ji LL, Herb RA, and Dudley G**.
607   Regional training-induced alterations in diaphragmatic oxidative and antioxidant
608   enzymes. *Respir Physiol* 95: 227-237, 1994.

609   40.   **Powers SK, Hudson MB, Nelson WB, Talbert EE, Min K, Szeto HH, Kavazis**
610   **AN, and Smuder AJ**. Mitochondria-targeted antioxidants protect against mechanical
611   ventilation-induced diaphragm weakness. *Crit Care Med* 39: 1749-1759, 2011.

612   41.   **Powers SK, Wiggs MP, Sollanek KJ, and Smuder AJ**. Ventilator-induced
613   diaphragm dysfunction: cause and effect. *American journal of physiology Regulatory,*
614   *integrative and comparative physiology* 305: R464-477, 2013.

615   42.   **Riley DA, Bain JL, Thompson JL, Fitts RH, Widrick JJ, Trappe SW, Trappe**
616   **TA, and Costill DL**. Disproportionate loss of thin filaments in human soleus muscle after
617   17-day bed rest. *Muscle Nerve* 21: 1280-1289, 1998.

618   43.   **Roberts BM, Ahn B, Smuder AJ, Al-Rajhi M, Gill LC, Beharry AW, Powers SK,**
619   **Fuller DD, Ferreira LF, and Judge AR**. Diaphragm and ventilatory dysfunction during

cancer cachexia. *FASEB journal : official publication of the Federation of American Societies for Experimental Biology* 27: 2600-2610, 2013.

44.   **Schuler M, Ali F, Metzger E, Chambon P, and Metzger D**. Temporally controlled targeted somatic mutagenesis in skeletal muscles of the mouse. *Genesis* 41: 165-170, 2005.

45.   **Shanely RA, Van Gammeren D, Deruisseau KC, Zergeroglu AM, McKenzie MJ, Yarasheski KE, and Powers SK**. Mechanical ventilation depresses protein synthesis in the rat diaphragm. *Am J Respir Crit Care Med* 170: 994-999, 2004.

46.   **Siafakas NM, Jordan M, Wagner H, Breen EC, Benoit H, and Wagner PD**. Diaphragmatic angiogenic growth factor mRNA responses to increased ventilation caused by hypoxia and hypercapnia. *Eur Respir J* 17: 681-687, 2001.

47.   **Simonini A, Massie BM, Long CS, Qi M, and Samarel AM**. Alterations in skeletal muscle gene expression in the rat with chronic congestive heart failure. *J Mol Cell Cardiol* 28: 1683-1691, 1996.

48.   **Supinski GS, Wang W, and Callahan LA**. Caspase and calpain activation both contribute to sepsis-induced diaphragmatic weakness. *J Appl Physiol (1985)* 107: 1389-1396, 2009.

49.   **Taimeh Z, Loughran J, Birks EJ, and Bolli R**. Vascular endothelial growth factor in heart failure. *Nat Rev Cardiol* 10: 519-530, 2013.

50.   **Tang K, Gu Y, Dalton ND, Wagner H, Peterson KL, Wagner PD, and Breen EC**. Selective Life-Long Skeletal Myofiber-Targeted VEGF Gene Ablation Impairs Exercise Capacity in Adult Mice. *Journal of cellular physiology* 231: 505-511, 2016.

51.   **Tang K, Rossiter HB, Wagner PD, and Breen EC**. Lung-targeted VEGF inactivation leads to an emphysema phenotype in mice. *J Appl Physiol* 97: 1559-1566; discussion 1549, 2004.

52.   **Tang K, Wagner PD, and Breen EC**. TNF-alpha-mediated reduction in PGC-1alpha may impair skeletal muscle function after cigarette smoke exposure. *Journal of cellular physiology* 222: 320-327, 2010.

53.   **van Hees HW, Ottenheijm CA, Granzier HL, Dekhuijzen PN, and Heunks LM**. Heart failure decreases passive tension generation of rat diaphragm fibers. *Int J Cardiol* 141: 275-283, 2010.

Figure Legends

653 **Figure 1.** Diaphragm contractile function in skeletal muscle-specific VEGF deficient (skmVEGF$^{-/-}$

654) mice compared to wild type (WT) controls. Isolated diaphragm fiber bundles were stimulated at

655 increasing stimulation frequencies to measure isometric specific force (**A**) and normalized relative

656 to maximum force **(B),** with fatigability assessed during repeated stimulations (**C**). Data are

657 mean±SD. *P<0.01; §P<0.05 skmVEGF$^{-/-}$ vs WT.

658

659 **Figure 2.** Diaphragm structural properties in skeletal muscle specific-VEGF deficient (skmVEGF^{-}

660 $^{/-}$) mice compared to wild type (WT) controls, which included assessment of capillary-to-fiber (C/F)

661 ratio (**A**), capillary density (CD) (**B**), and mean fiber cross-sectional area (FCSA) (**C**) (n = 5 per

662 group). Representative immunofluorescent diaphragm sections from WT (**D**) and skmVEGF$^{-/-}$ (**E**)

663 mice (fiber boundaries stained red, type I fibers green, and type II fibers unstained), revealed no

664 change in fiber type proportions (**F**) but a type I specific fiber atrophy in skmVEGF$^{-/-}$ mice

665 compared to WT controls (n = 8-11 per group). Data are presented as mean±SD. *P<0.05

666 skmVEGF$^{-/-}$ vs WT.

667

668 **Figure 3.** Protein expression in the diaphragm of the key contractile proteins myosin heavy chain

669 (MyHC; **A**) and sarcomeric actin (**B**), as well as respective representative blots (**C**) in skeletal

670 muscle-specific VEGF deficient (skmVEGF$^{-/-}$) mice compared to wild type (WT) controls. Data

671 were normalized to the loading control GAPDH and calculated as fold change (Δ) vs. WT. Data

672 are presented as mean±SD. *P=0.01 skmVEGF$^{-/-}$ vs WT.

673

674 **Figure 4.** Diaphragm protein expression along with representative blots of regulatory muscle

675 signalling proteins measured in skeletal muscle-specific VEGF deficient (skmVEGF$^{-/-}$) mice

676 compared to wild type (WT) controls, which included the key atrogin MAFBx (**A**) and ROS source

677 NADPH oxidase (subunit gp91^{phox}) (**B**), as well as the upstream VEGF activators HIF-1α (**C**) and

25

678   PGC-1α (**D**). Data were normalized to the loading control GAPDH and calculated as fold change

679   (Δ) vs. WT. Data are presented as mean±SD.

680

681   **Figure 5.** Diaphragm mitochondrial respiratory function and ROS production. Rate of oxygen

682   consumption (JO_2) measured during a high-resolution respirometry substrate-uncoupler-inhibitor-

683   titration (SUIT) protocol. **Panel A:** LEAK: glutamate+malate for LEAK state respiration.

684   OXPHOS_CI: ADP for the phosphorylating state with substrates provided to complex I.

685   OXPHOS_CI+II: ADP+succinate. ETS: Carbonyl cyanide m-chlorophenyl hydrazine for

686   uncoupled respiration and electron transport system capacity. ETS_CII: Rotenone added to inhibit

687   complex I. **Panel B:** H_2O_2 flux measured simultaneous to JO_2. Main effect of genotype present

688   ($F_{[1, 75]} = 14.57$, P=0.0003) and * denotes different to WT. **Panel C:** OXPHOS coupling efficiency

689   was calculated as (1-LEAK / OXPHOS_CI+II). **Panel D:** Flux control ratio (FCR) for OXPHOS_CI

690   was calculated as (OXPHOS_CI / ETS). **Panel E:** FCR for OXPHOS_CI+II was calculated as

691   (OXPHOS_CI+II / ETS). **Panel F:** Substrate control ratio (SCR) for succinate was calculated as

692   (OXPHOS_CI+II / OXPHOS_CI). Error bars are SD, n=8-10.
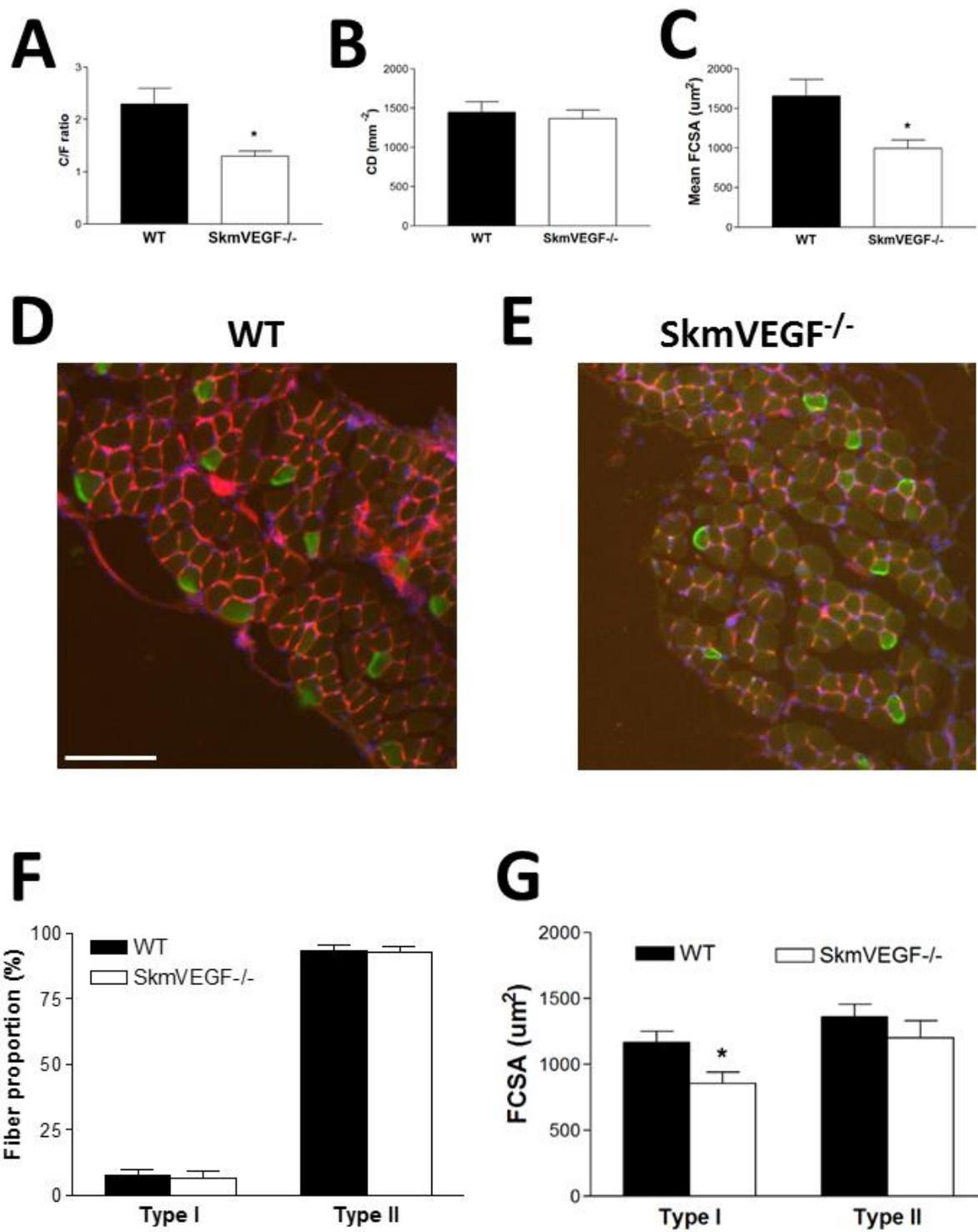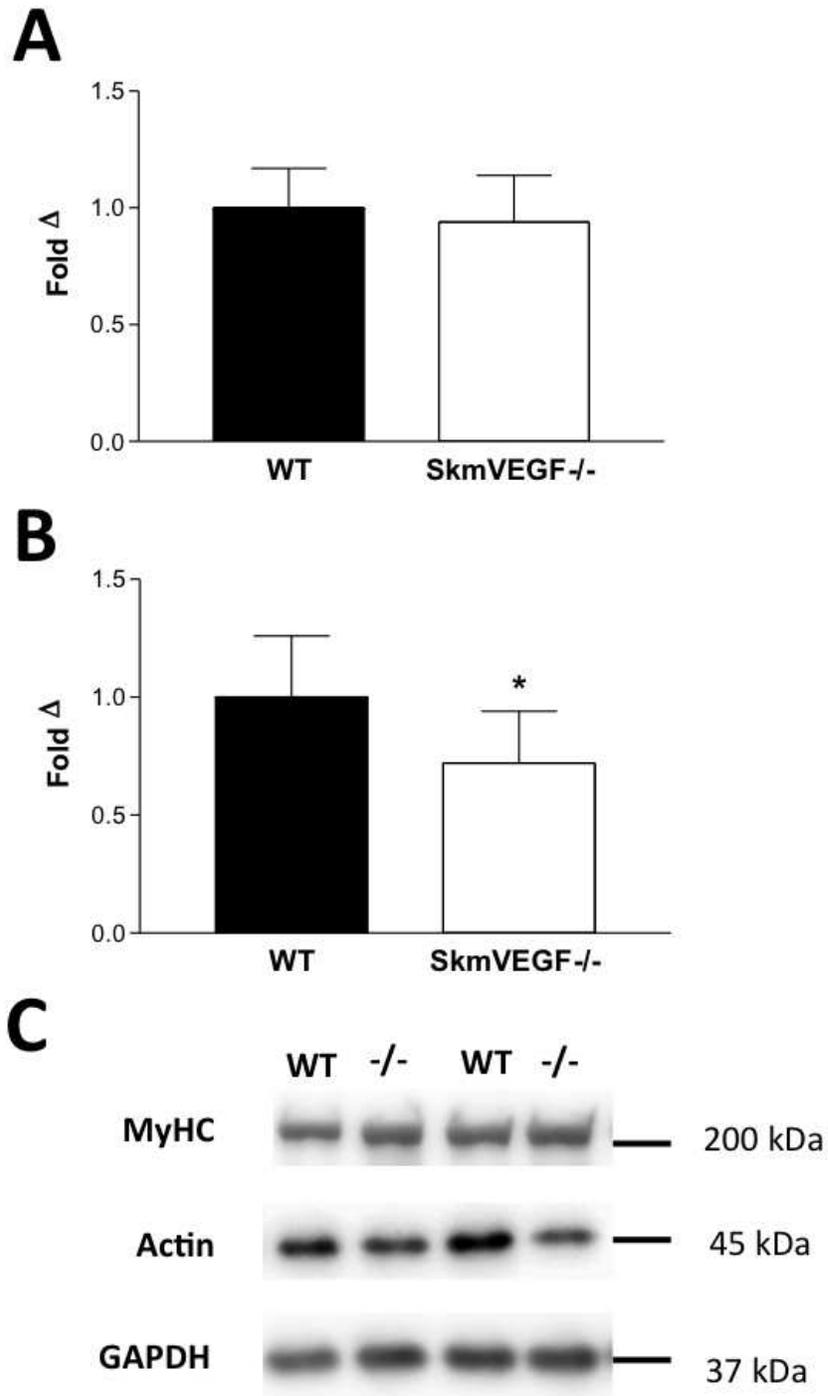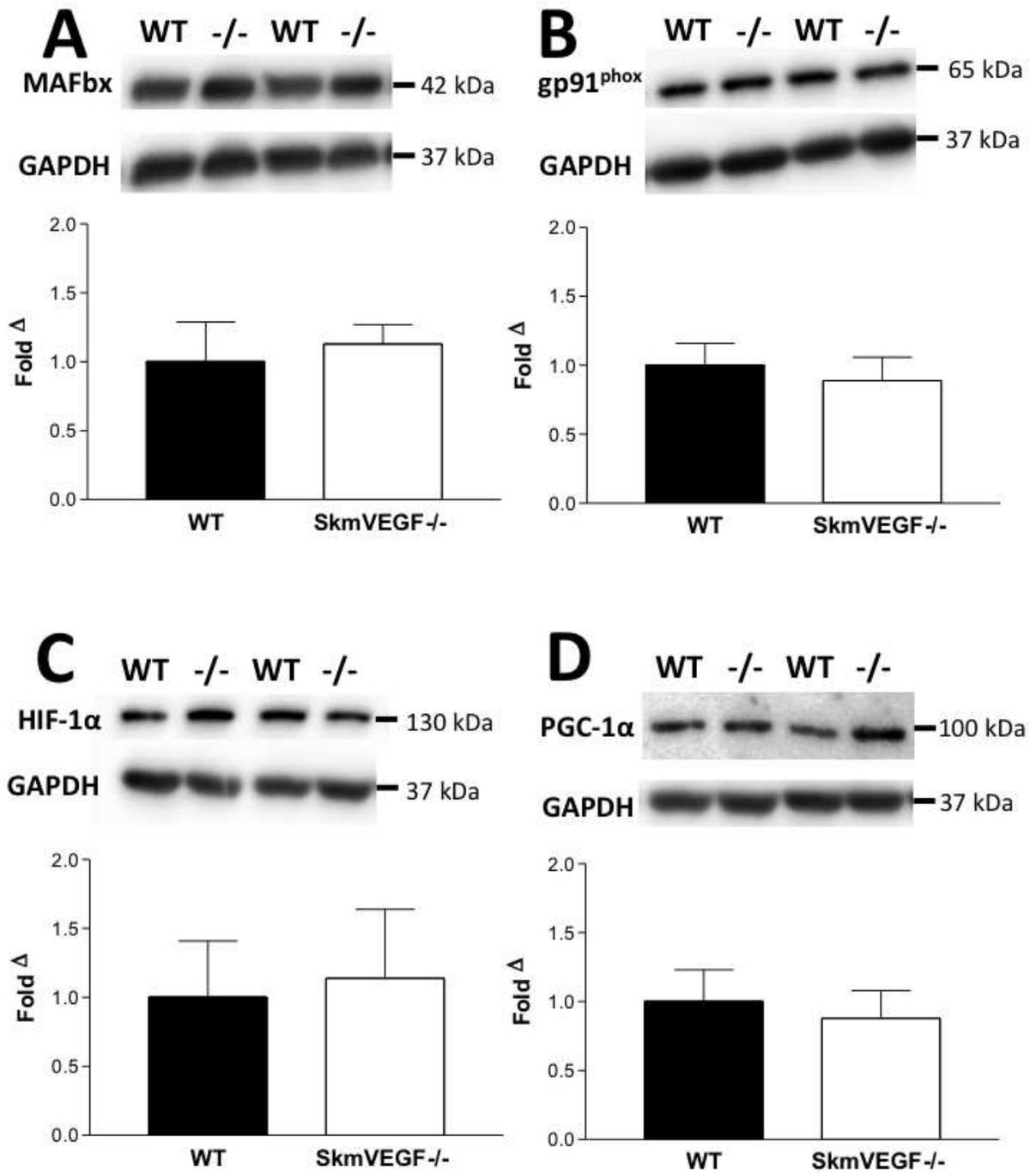
693
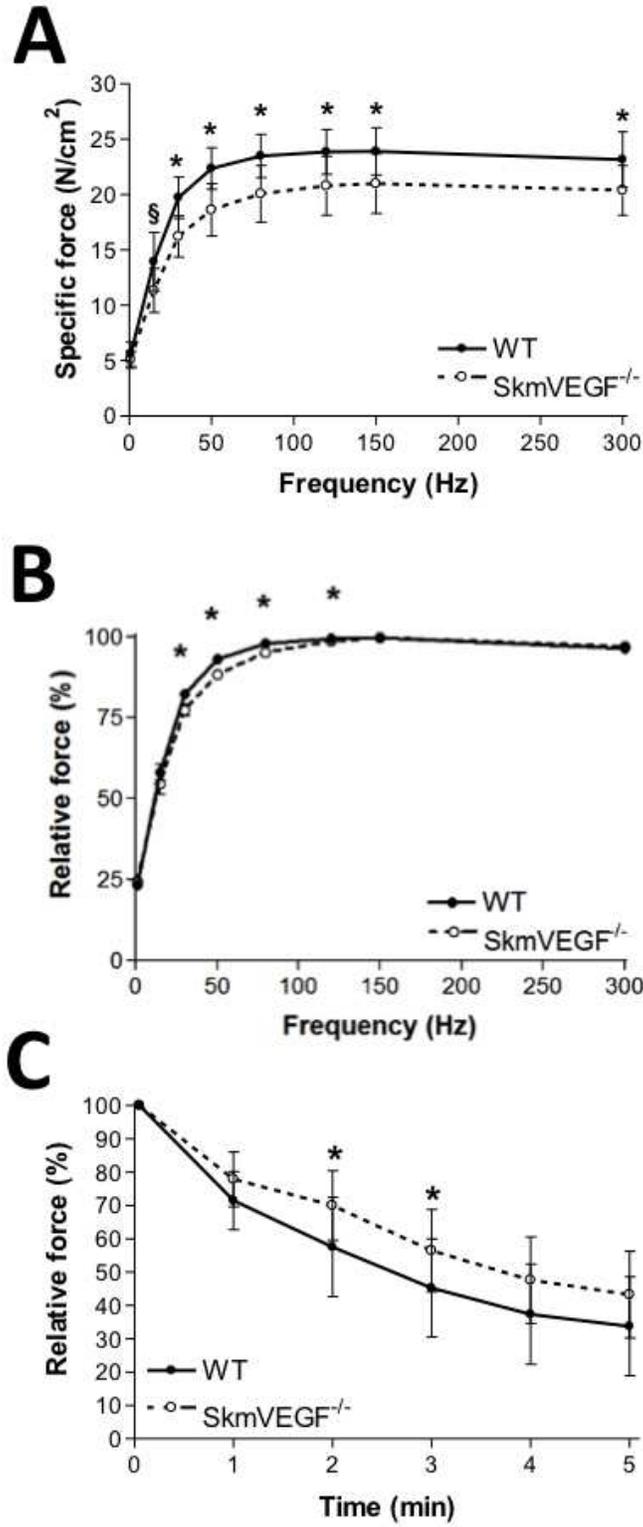
694

695 **Figure 1.**
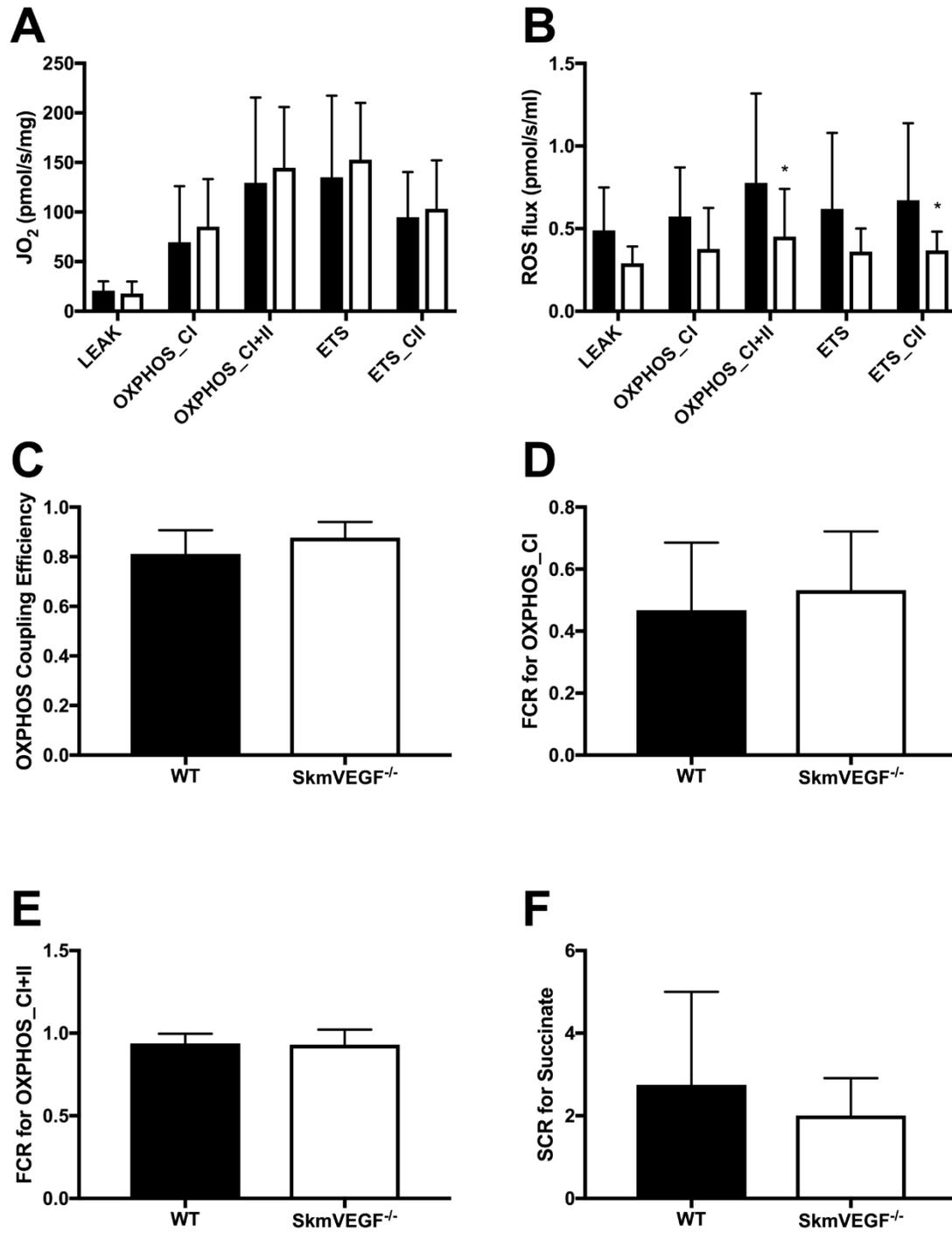
696

697

698 **Figure 2.**

699

700

Figure 3.

702

703

Figure 4.

705

706

707   **Figure 5.**

708